Front. Earth Sci. 2023, 17(2): 505−513
https://doi.org/10.1007/s11707-022-1017-y

RESEARCH ARTICLE

Amplitude variation with offset and azimuth inversion to predict and evaluate coal seam fracture parameters

Haibo WU (✉)[1,2], Shujie ZHU[3], Qinjie LIU[2], Shouhua DONG[4], Yanhui HUANG[1,5], Pingsong ZHANG[1]

1 School of Earth and Environment, Anhui University of Science and Technology, Huainan 232001, China
2 Institute of Energy, Hefei Comprehensive National Science Center (Anhui Energy Laboratory), Hefei 230051, China
3 Xi'an Research Institute, China Coal Technology & Engineering Group, Xi'an 710076, China
4 School of Resources and Geosciences, China University of Mining and Technology, Xuzhou 221116, China
5 State Key Laboratory of Petroleum Resources and Prospecting, China University of Petroleum, Beijing 102249, China

Abstract Amplitude variation with offset and azimuth (AVOA) inversion is a mainstream method for predicting and evaluating fracture parameters of conventional oil and gas reservoirs. However, its application to coal seams is limited because of the specificity of the equivalent media model for coal—also, the traditional seismic acquisition system employed in coal fields falls within a narrow azimuth. In this study, we initially derived a P–P wave reflection coefficient approximation formula for coal seams, which is directly expressed in terms of fracture parameters using the Schoenberg linear-slide model and Hudson model. We analyzed the P–P wave reflection coefficient's response to the fracture parameters using a two-layer forward model. Accordingly, we designed a two-step inversion workflow for AVOA inversion of the fracture parameters. Thereafter, high-density wide-azimuth pre-stack 3D seismic data were utilized for inverting the fracture density and strike of the target coal seam. The inversion accuracy was constrained by Student's *t*-distribution testing. The analysis and validation of the inversion results revealed that the relative fracture density corresponds to fault locations, with the strike of the fractures and faults mainly at 0°. Therefore, the AVOA inversion method and technical workflow proposed here can be used to efficiently predict and evaluate fracture parameters of coal seams.

Keywords equivalent media model, fracture density and strike, azimuth, Student's *t*-distribution

1 Introduction

Accurate identification of coal-bed methane (CBM)-rich areas is vital for successful CBM exploitation. These CBM-rich areas must satisfy two basic conditions to ensure profitable extraction: high gas content and elevated permeability (Chen et al., 2014). Unfortunately, most coal seams in China cannot meet both conditions, especially that of high permeability. Therefore, the delineation of high-permeability areas requires attention. The development of a natural fracture system in a coal field usually has a positive effect on the permeability (Fu et al., 2007). Predicting the natural fracture parameters before evaluating the permeability of a coal seam is valuable for guiding the reservoir fracturing and exploitation design.

Recently, the amplitude variation with offset and azimuth (AVOA) inversion method has become a commonly applied solution for predicting fracture parameters and evaluating conventional hydrocarbon reservoirs. This method was introduced by Mallick et al. (1998) and employed to qualitatively evaluate the density and strike of fractures. To reduce the inversion error associated with the method, Shen et al. (2002) proposed extracting the frequency variation with offset attributes and using only the amplitude in the inversion. Thereafter, many studies focused on the prediction accuracy of the AVOA inversion method. Further, Hall and Kendall (2003) introduced a surface fitting method for optimizing the traditional AVOA inversion, with forward modeling used to constrain the inversion. In addition, Luo and Evans (2003, 2004) evaluated the influence of the anisotropy characteristics of the upper medium through physical modeling and real data, reporting improved inversion accuracy for the fracture parameters of the target reservoir. Duxbury et al. (2012) inverted the anisotropic gradient of a target reservoir using the AVOA method, and the results were consistent with the corresponding data collected from drilling and logging.

Received November 23, 2021; accepted April 25, 2022

E-mail: wuhaibocumt@163.com

In coal-field seismic exploration, amplitude variation with offset (AVO) inversion has been applied for detecting features such as CBM-enriched areas and water-bearing limestone reservoirs (Peng et al., 2006, 2014; Wu et al., 2015, 2016, 2020; Tian et al., 2017). However, the application of this method thus far neglects the anisotropic characteristics of coal seams. Accordingly, some researchers have focused on optimizing AVOA for use in the coalfield. Ramos and Davis (1997) conducted one of the most representative studies by using the traditional AVOA method to invert the fracture parameters of coal seams. In addition, Dong (2004) and Chen et al. (2010) studied the AVOA responses of horizontal transverse isotropic (HTI) coal seams. Deng et al. (2010) proposed an AVOA forward method for anisotropic thin coal seams. Moreover, Peng et al. (2013) utilized the AVOA response of the fracture parameters of a coal seam for evaluating the distribution of tectonic coal.

Currently, anisotropy caused by fractures can be analyzed by seismic inversion to discover unconventional reservoirs; however, this strategy remains to be applied in coalfields. Referring to the successful cases of conventional hydrocarbon reservoirs is a reasonable approach to optimizing the AVOA inversion method for predicting and evaluating coal seam fracture parameters. However, the peculiarity of the coal seam equivalent media model in fluid and anisotropy expressions must be considered in advance, and a wide-azimuth observation system during seismic exploration is required. Therefore, in this study, we initially derived the P–P wave reflection coefficient approximation formula involving fracture parameters. Next, we designed a two-step inversion flow for a coal seam using the Schoenberg linear-slide model and Hudson model, while considering the fracture fluid characteristics. Then, we conducted an inversion case study based on high-density wide-azimuth pre-stack 3D seismic data, with the inversion accuracy constrained by the Student's *t*-distribution test. Finally, we discuss the inversion results and the impact of the method.

2 Method

2.1 Coal seam equivalent media model

Generally, a coal seam is affected by tectonic stress and overburden pressure almost horizontally and vertically, respectively. Horizontal fractures are often sealed by compaction from the overburden pressure, while the vertical fractures remain open. These can be described as fluid-filled penny-shaped fractures within isotropic coal and can be determined by the HTI media model, showing azimuthal anisotropic characteristics in the seismic wave propagation (Sun et al., 2014). According to the Schoenberg linear-slide model (Schoenberg and Sayers, 1995), the stiffness matrix C can be expressed as follows:

$$
\begin{aligned}
C &= \begin{bmatrix}
C_{11} & C_{13} & C_{13} & 0 & 0 & 0 \\
C_{13} & C_{33} & C_{23} & 0 & 0 & 0 \\
C_{13} & C_{23} & C_{33} & 0 & 0 & 0 \\
0 & 0 & 0 & C_{44} & 0 & 0 \\
0 & 0 & 0 & 0 & C_{66} & 0 \\
0 & 0 & 0 & 0 & 0 & C_{66}
\end{bmatrix} \\
&= \begin{bmatrix}
(\lambda+2\mu)(1-\Delta_N) & \lambda(1-\Delta_N) & \lambda(1-\Delta_N) & 0 & 0 & 0 \\
\lambda(1-\Delta_N) & (\lambda+2\mu)(1-\chi^2\Delta_N) & \lambda(1-\chi\Delta_N) & 0 & 0 & 0 \\
\lambda(1-\Delta_N) & \lambda(1-\chi\Delta_N) & (\lambda+2\mu)(1-\chi^2\Delta_N) & 0 & 0 & 0 \\
0 & 0 & 0 & \mu & 0 & 0 \\
0 & 0 & 0 & 0 & \mu(1-\Delta_T) & 0 \\
0 & 0 & 0 & 0 & 0 & \mu(1-\Delta_T)
\end{bmatrix},
\end{aligned}
\tag{1}
$$

where C_{ij} denote the elastic constants. Five independent elastic constants are required to describe the HTI media. In Eq. (1), $\chi = \dfrac{\lambda}{\lambda+2\mu}$, λ, and μ are the Lamé constants; and Δ_N and Δ_T are the normal and tangential fracture weaknesses, respectively.

By combining the Schoenberg linear-slide model and Hudson model (Schoenberg and Douma, 1988), Δ_N and Δ_T can be expressed in Eq. (2) as follows:

$$
\begin{cases}
\Delta_N = \dfrac{\lambda+2\mu}{\mu} U_{33} e \\
\Delta_T = U_{11} e
\end{cases},
\tag{2}
$$

where U_{11} and U_{33} are parameters in the Hudson model dependent on the fracture style (Mavko et al., 1998), $e = \dfrac{3\phi}{4\pi\alpha}$ denotes the fracture density, ϕ is the fracture porosity, and α represents the fracture aspect ratio. The terms U_{11} and U_{33} are expressed according to the fracture styles (Hudson, 1981), and are expressed for a dry fracture as follows:

$$
\begin{cases}
U_{11} = \dfrac{16(\lambda+2\mu)}{3(3\lambda+4\mu)} \\
U_{33} = \dfrac{4(\lambda+2\mu)}{3(\lambda+\mu)}
\end{cases}.
\tag{3}
$$

For penny-shaped and fluid-filled fractures, these are given as follows:

$$\begin{cases} U_{11} = \dfrac{16(\lambda+2\mu)}{3(3\lambda+4\mu)} \\ U_{33} = 0 \end{cases}. \tag{4}$$

During coal field exploration, coal seam fractures are mostly saturated with water. Therefore, by substituting Eq. (4) into Eq. (2), the latter can be rewritten as follows:

$$\begin{cases} \Delta_N = 0 \\ \Delta_T = \dfrac{16e}{3(3-2g)} \end{cases}, \tag{5}$$

where $g = \dfrac{\mu}{\lambda+2\mu} = \dfrac{V_S^2}{V_P^2}$. Then, we can express C_{ij} by Eq. (6):

$$\begin{cases} C_{11} = \lambda+2\mu \\ C_{33} = \lambda+2\mu \\ C_{13} = \lambda \\ C_{44} = \mu \\ C_{66} = \mu\left(1-\dfrac{16e}{3(3-2g)}\right) \end{cases}. \tag{6}$$

Finally, the anisotropic coefficients can be expressed by the fracture density of the coal seam, given in Eq. (7) (Bakulin et al., 2000), as

$$\begin{cases} \varepsilon^{(V)} = \dfrac{C_{11}-C_{33}}{2C_{33}} = 0 \\ \gamma^{(V)} = \dfrac{C_{66}-C_{44}}{2C_{44}} = -\dfrac{8e}{3(3-2g)} \\ \delta^{(V)} = \dfrac{(C_{13}+C_{66})^2-(C_{33}-C_{66})^2}{2C_{33}(C_{33}-C_{66})} = -\dfrac{32ge}{3(3-2g)} \end{cases}. \tag{7}$$

2.2 AVOA inversion equation

The P–P wave reflection coefficient approximation equation for an HTI medium (Rüger, 1997, 1998) can be expressed as follows:

$$\begin{aligned} R_{PP}(\theta,\varphi) &= \frac{1}{2}\frac{\Delta Z}{\overline{Z}} + \frac{1}{2}\left\{\frac{\Delta V_P}{\overline{V_P}} - \left(\frac{2\overline{V_S}}{\overline{V_p}}\right)^2\frac{\Delta G}{\overline{G}}\right. \\ &\left. + \left[\Delta\delta^{(V)} + 2\left(\frac{2\overline{V_S}}{\overline{V_p}}\right)^2\Delta\gamma^{(V)}\right]\cos^2\varphi\right\}\sin^2\theta \\ &+ \frac{1}{2}\left\{\frac{\Delta V_P}{\overline{V_P}} + \Delta\varepsilon^{(V)}\cos^4\varphi + \Delta\delta^{(V)}\sin^2\varphi\cos^2\varphi\right\}\sin^2\theta\tan^2\theta, \end{aligned} \tag{8}$$

where θ is the incident angle, φ denotes the shooting direction with respect to the strike of the fractures, $Z = \rho V_P$ represents the vertical impedance of the P-wave, $G = \rho V_S^2$ is the vertical shear modulus, with $\overline{V_P} = (V_{P2}+V_{P1})/2$, $\overline{V_S} = (V_{S2}+V_{S1})/2$, $\Delta V_P = V_{P2}-V_{P1}$, $\Delta V_S = V_{S2}-V_{S1}$, $\Delta\varepsilon^{(V)} = \varepsilon_2^{(V)} - \varepsilon_1^{(V)}$, $\Delta\gamma^{(V)} = \gamma_2^{(V)} - \gamma_1^{(V)}$, and $\Delta\delta^{(V)} = \delta_2^{(V)} - \delta_1^{(V)}$. The subscripts $_1$ and $_2$ represent the medium above and below the reflection interface, respectively.

For a small angle of incidence ($\alpha < 30°$), the high-order term in Eq. (8) can be approximated as following:

$$\begin{aligned} R_{PP}(\theta,\varphi) &= \frac{1}{2}\frac{\Delta Z}{\overline{Z}} + \frac{1}{2}\left\{\frac{\Delta V_P}{\overline{V_P}} - \left(\frac{2\overline{V_S}}{\overline{V_p}}\right)^2\frac{\Delta G}{\overline{G}}\right. \\ &\left. + \left[\Delta\delta^{(V)} + 2\left(\frac{2\overline{V_S}}{\overline{V_p}}\right)^2\Delta\gamma^{(V)}\right]\cos^2\varphi\right\}\sin^2\theta. \end{aligned} \tag{9}$$

By substituting Eq. (7) into Eq. (9), the P–P wave reflection coefficient can be expressed directly through the fracture density given in Eq. (9) as following:

$$R_{PP}(\theta,\varphi) = \frac{1}{2}\frac{\Delta Z}{\overline{Z}} + \frac{1}{2}\left\{\frac{\Delta V_P}{\overline{V_P}} - 4\bar{g}\frac{\Delta G}{\overline{G}} + \frac{32\bar{g}\Delta e}{3(3-2\bar{g})}\cos^2\varphi\right\}\sin^2\theta. \tag{10}$$

By simplifying Eq. (10), Eq. (11) can be obtained and given as follows:

$$\begin{cases} R_{PP}(\theta,\varphi) = A + B(\varphi)\sin^2\theta \\ B(\varphi) = G_{\text{iso}} + G_{\text{ani}}\cos^2\varphi \end{cases}, \tag{11}$$

where $A = \dfrac{\Delta Z}{2\overline{Z}}$ is the intercept term, $B(\varphi)$ represents the gradient term, $G_{\text{iso}} = \dfrac{\Delta V_P}{2\overline{V_P}} - 2\bar{g}\dfrac{\Delta G}{\overline{G}}$ denotes the isotropic gradient term, and $G_{\text{ani}} = \dfrac{16\bar{g}\Delta e}{3(3-2\bar{g})}$ is the anisotropic gradient term. Generally, the $\bar{g}$ of rocks in an area are relatively unaltered and can be assessed by the logs. Evidently, a positive correlation exists between the anisotropic gradient term (G_{ani}) and the relative fracture density (Δe), and φ can be used to directly indicate the fracture strike.

2.3 P–P wave reflection coefficient responses to the fracture parameters

A two-layer forward model with an HTI fracture coal seam below the reflection surface is shown in Fig. 1. The roof of the coal seam is isotropic mudstone; P-wave

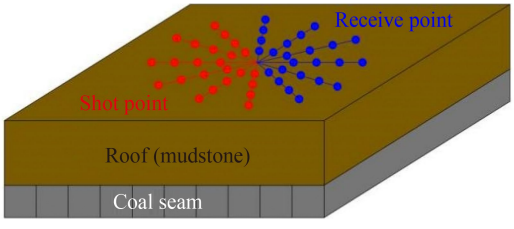

Fig. 1 Two-layer forward model with a horizontal transverse isotropic (HTI) fracture coal seam below the reflection surface.

velocity, S-wave velocity, and density are equal to 3.0 km/s, 2.0 km/s, and 2.3 g/cm^3, respectively. The vertical velocities of the P and S waves of coal seam are equal to 2.59 km/s and 1.35 km/s, respectively. The density of the coal seam is equal to 1.44 g/cm^3.

The P–P wave reflection coefficient responses to the fracture parameters are shown in Fig. 2. The P–P wave reflection coefficients do not show the azimuthal anisotropy when the P-wave incident to the interface is vertical, with θ equal to 0° (Fig. 2(a)). In Figs. 2(b), 2(c), and 2(d), stronger azimuthal anisotropy of the P–P wave reflection coefficients were exhibited with increasing θ or fracture density.

3 Inversion method and error analysis

3.1 Two-step inversion workflow

According to the AVOA inversion equation given in Eq. (11), the coal seam fracture parameter inversion was conducted in the following two steps.

First, super-gathers were extracted from the pre-stack azimuthal angle gathers, and then the gradient term ($B(\varphi)$) was calculated for each super-gather by linear fitting according to $R_{PP}(\theta,\varphi) = A + B(\varphi)\sin^2\theta$.

Next, the anisotropic gradient term (G_{ani}), fracture strike (β), and inversion error (err) for each super-gather were calculated by fitting $B(\varphi)$, and then the relative fracture density (Δe) was obtained.

The unknown terms φ and β are required to solve the inversion equation ($B(\varphi) = G_{\text{iso}} + G_{\text{ani}}\cos^2\varphi$) by least-squares ellipse fitting. For this, Eq. (11) can be rewritten (Grechka and Tsvankin, 1998; Jenner, 2002) as follows:

$$B(\varphi) = W_{11}\cos^2\varphi' + 2W_{12}\sin\varphi'\cos\varphi' + W_{22}\sin^2\varphi', \quad (12)$$

where φ' is the azimuth set in the acquisition system. Thereafter, the anisotropic gradient term and fracture strike can be calculated through W_{ij} given in Eq. (13) as follows:

$$\begin{cases} G_{\text{ani}} = \sqrt{(W_{11}-W_{22})^2 + 4W_{12}^2} \\ \beta = \arctan\left[\dfrac{W_{22}-W_{11}+\sqrt{(W_{11}-W_{22})^2+4W_{12}^2}}{2W_{12}}\right] \end{cases}. \quad (13)$$

3.2 Error analysis method

Generally, error propagation occurs in the ellipse fitting procedure, and the probability distribution of this error follows the derivative chain rule (Xia et al., 2006). Beers (1962) proposed an error propagation formula expressed as follows:

$$S_n = \sqrt{\left(\frac{\partial n}{\partial x}\right)^2 S_x^2 + \left(\frac{\partial n}{\partial y}\right)^2 S_y^2 + \left(\frac{\partial n}{\partial z}\right)^2 S_z^2 + \cdots}, \quad (14)$$

where S_x, S_y, and S_z are the standard deviations of x, y, and z, respectively. The standard deviation of the anisotropic gradient term can then be expressed as follows:

$$S_{G_{\text{ani}}} = \frac{\sqrt{(W_{11}-W_{22})^2(S_{W_{11}}^2 + S_{W_{22}}^2) + 16W_{12}^2 S_{W_{12}}^2}}{G_{\text{ani}}}, \quad (15)$$

where $S_{W_{ij}}$ is the standard deviation of W_{ij}. Student's t-test value can be calculated as follows:

$$t = \frac{G_{\text{ani}}}{S_{G_{\text{ani}}}}. \quad (16)$$

The accuracy of the inversion results can be evaluated by calculating the t of the target reservoir in the surveyed area and providing a critical t (t_α) value corresponding to the set confidence interval. If $t \leqslant t_\alpha$, the inversion result should be rejected for the set confidence interval, whereas

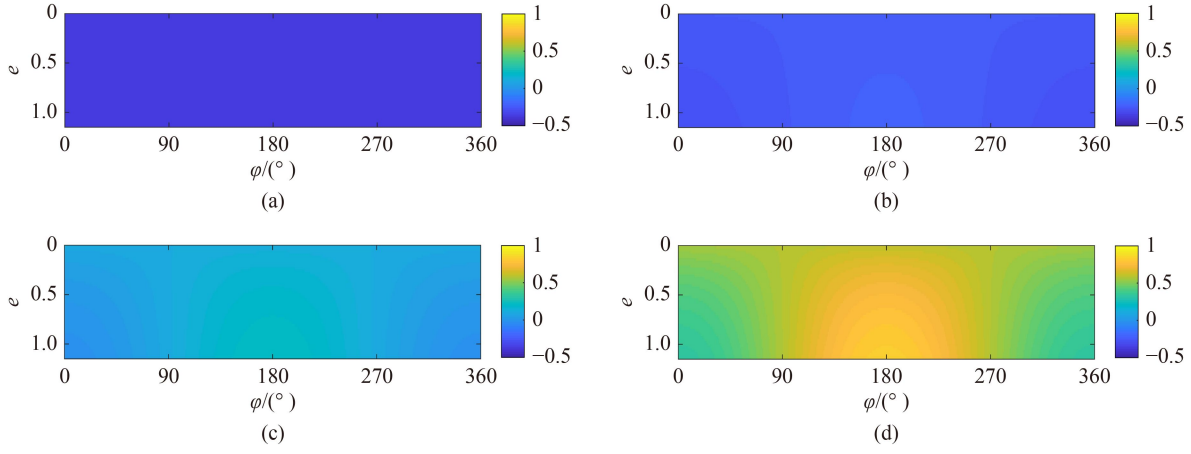

Fig. 2 P–P wave reflection coefficient responses to the fracture density at different incidence angles and azimuths. (a) θ is equal to 0°; (b) θ is equal to 15°; (c) θ is equal to 30°; (d) θ is equal to 45°.

when $t > t_\alpha$, the inversion result is acceptable (Xia et al., 2006).

By integrating the two-step inversion workflow and Student's *t*-distribution test for the inversion results, we summarized the AVOA inversion workflow for the coal seam fracture parameters (Fig. 3).

4 Coal seam fracture parameters: an AVOA inversion case study

4.1 Overview of the survey area

The approximately 1.6 km^2 area in the Ordos Basin surveyed is displayed in Fig. 4. In Fig. 5, a typical lithologic column of the area, comprising the Taiyuan Formation (C3t) and Shanxi Formation (P1s) of the Carboniferous and Permian coal series, is shown. The No. 6 coal seam, representing the target, is at the top of the Taiyuan Formation, with thicknesses ranging from 7.04 to 20.77 m and an average of 12.70 m. Above the coal seam, coarse and fine sandstones are common, while mudstones and sandy mudstones are prevalent below the seam, with some coarse sandstones.

4.2 Parameters of the seismic acquisition system

The high-density wide-azimuth bunched system utilized for the 3D seismic data acquisition is illustrated in Fig. 4. The dimensions and folds of each common-depth-point (CDP) bin were 5 m × 5 m and 8 (Inline) × 8 (Xline), respectively. The typical CDP gather after pre-migration shows that the two-way travel time of the reflected wave from the No. 6 coal seam is about 390 ms, with highlighted reflection events and a high signal-to-noise ratio, as depicted in Fig. 6.

4.3 Fracture parameter inversion results for the target coal seam

The W_{ij} is calculated by ellipse fitting of the gradient term of each super-gather according to Eq. (12), as shown in Fig. 7. Then, the anisotropic gradient term and fracture strike are computed based on Eq. (13).

The g values of the target coal seam and its overlying strata were 0.25 and 0.33, respectively, with a $\bar{g}$ value of 0.29 based on statistical analysis of the surveyed area logs. We referred to and set t_α to 1.333 for a 90% confidence interval. Then, the relative fracture density (Δe) was calculated and tested, with the results—and those of the calculated fracture strikes—shown in Fig. 8. The areas in white in Fig. 8 denote the inversion results t outside the confidence interval. The relative fracture density results increase from cyan to red, with the fracture strike denoted by short black lines. Figure 8 shows high

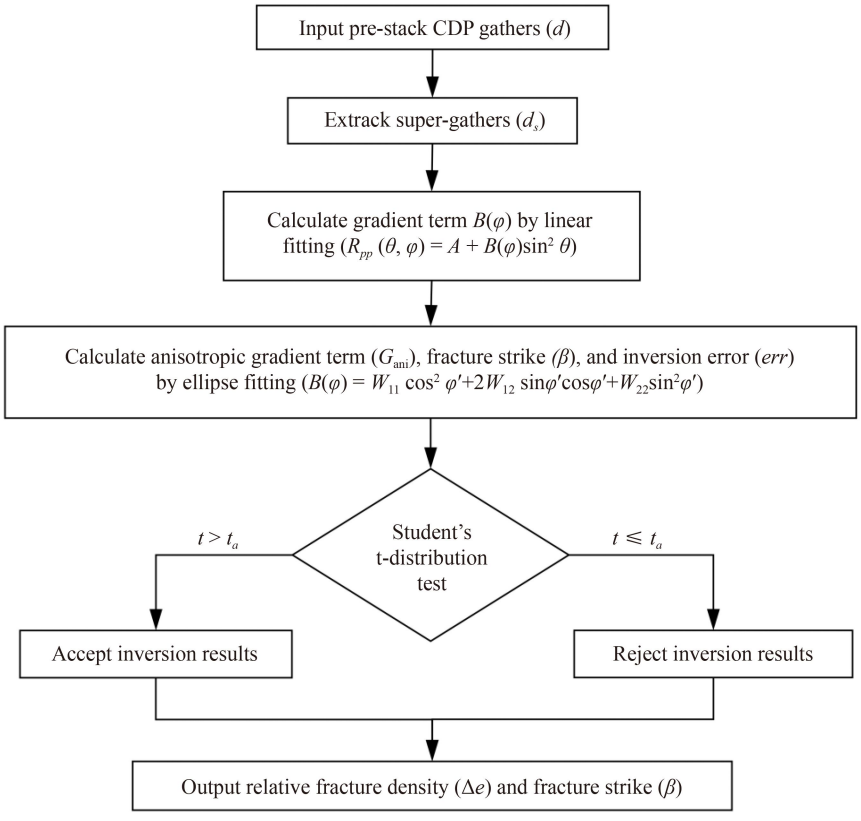

Fig. 3 Technical workflow involving the amplitude variation with offset and azimuth (AVOA) inversion for coal seam fracture parameters.

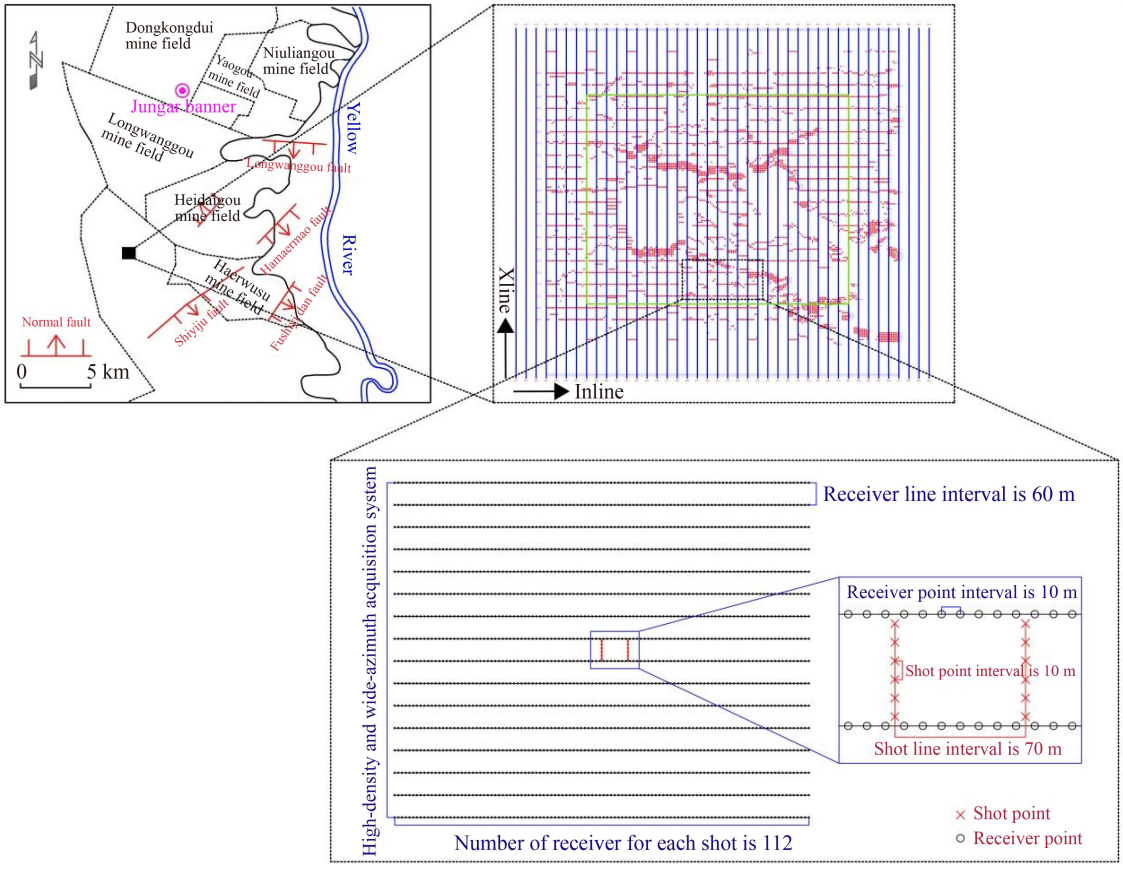

Fig. 4 Location, measure point distribution, and acquisition system parameters for the surveyed area.

relative fracture density values in the area with Inline numbers ranging from 300 to 500 and Xline numbers from 380 to 530, indicating the development of fractures.

The fracture strike data are displayed using a Rose diagram in Fig. 9, with the strikes mainly around 0° (north) and posteriorly around 90°.

4.4 Comparison of fracture parameter inversion and fault interpretation results

According to the projection of the fault interpretation results onto the fracture parameter inversion results (Fig. 8) in Fig. 10, apart from DF3 and DF5, most faults were within the fracture development areas. The data in Fig. 11 demonstrated that most faults in the surveyed area have a strike of 0°, which is consistent with the fracture strikes in Fig. 9. Overall, the fracture parameter inversion results display a satisfactory agreement with the fault interpretation results.

4.5 Discussion

A comparison of Figs. 4 and 10 reveals that the location of the measured point deficiency in Fig. 4 coincides with the locations where the inversion results are outside the confidence interval in Fig. 10. This result indicates that the complex surface conditions seriously affect the seismic data acquisition quality and, therefore, the accuracy of the fracture parameter inversion results. The fault interpretation results for DF3 and DF5 may be primarily influenced by this factor, although the limit scale is another factor that may account for the inconsistency between the interpretation of DF5 and the fracture parameter inversion results.

The absence of the formation micro-scanner logging information limited direct proof of the fracture parameter inversion results. Scale disunity exists when comparing the fracture with the fault because a fracture develops on a small scale, while a fault involves large scale displacement. This characteristic and the acquisition quality, affected by the complex surface conditions, explain the inconsistency between the fracture parameter inversion and the fault interpretation results.

Generally, multiple factors, such as folding, jointing, the sedimentary environment, and the covering lithology, may impact fracture development. However, in the study area, the simple geological structure, relatively unaltered sedimentary environment, and the lithology covering the survey area reduce the uncertainty associated with factors that influence the fractures. Therefore, a targeted acquisition system designed for pre-stack AVOA inversion coupled with high-quality data acquisition under complex surface conditions may efficiently enhance the accuracy of the fracture parameter inversion in the survey area.

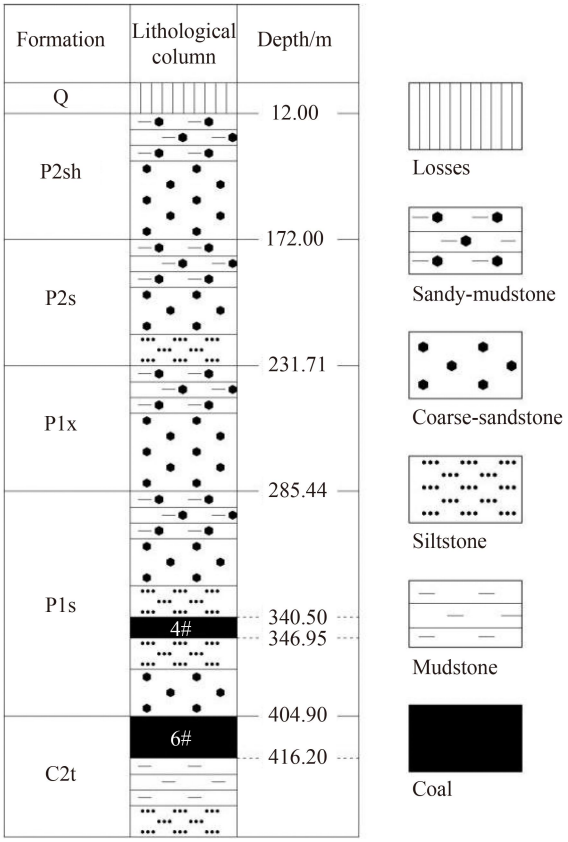

Fig. 5 Lithologic column of the surveyed area. No. 6 coal seam representing the target is at the top of the Taiyuan Formation (C2t).

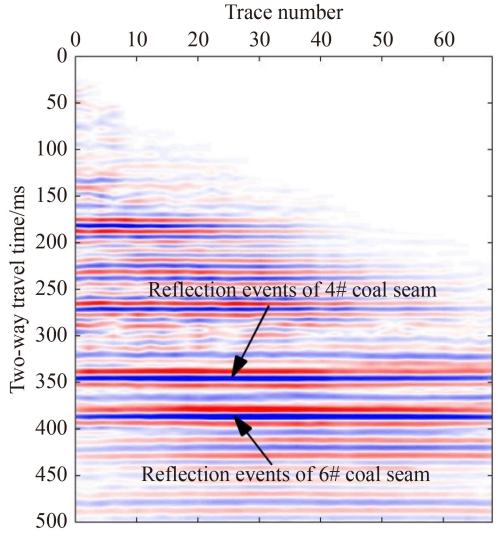

Fig. 6 Common-depth-point (CDP) gather displaying reflection events attributed to the target coal seam.

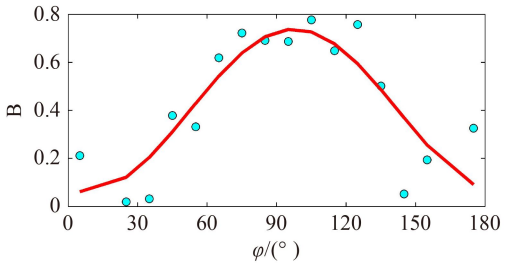

Fig. 7 Plot illustrating ellipse fitting of the gradient term. The cyan dots represent the value of the gradient term at different azimuths, and the red curve represents the fitting result.

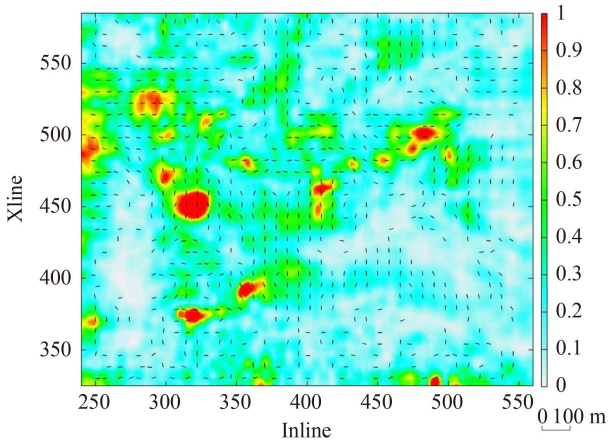

Fig. 8 Display of inversion results for the relative fracture density (Δe) and fracture strike (β). The colors denote the relative fracture density, while the short black lines represent the fracture strike.

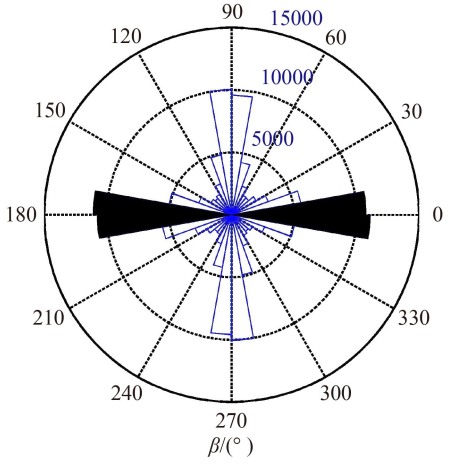

Fig. 9 Rose diagram displaying the fracture strike, with the numbers in black denoting the azimuth, and those in blue representing the fracture strike.

5 Conclusions

An AVOA inversion method for coal seam fracture parameters, driven by an equivalent media model and high-density wide-azimuth 3D pre-stack seismic data, was developed in this study. The principal findings are summarized as follows.

1) According to the fracture fluid characteristics of a coal seam, we derived a P–P wave reflection coefficient approximation formula for a coal seam, which directly

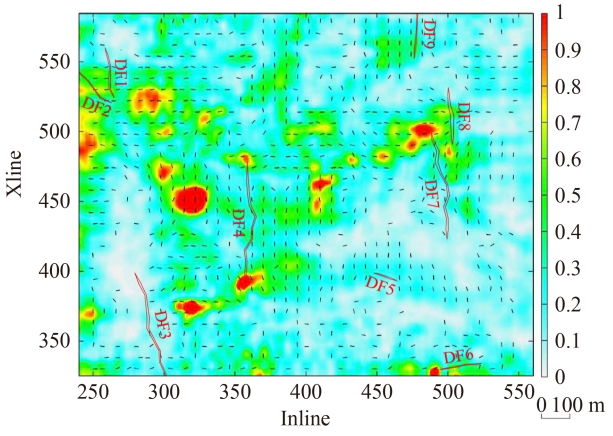

Fig. 10 Plot comparing the fracture parameter inversion and fault interpretation results.

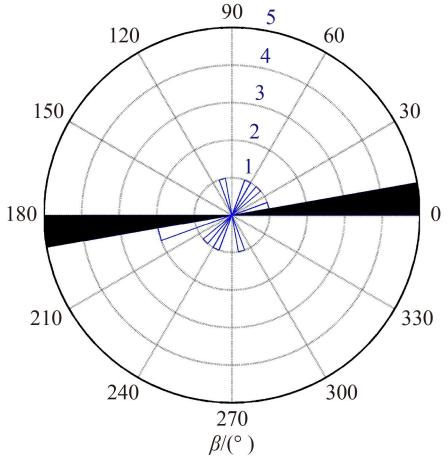

Fig. 11 Rose diagram displaying the fault strike data for the surveyed area. The numbers in black denote the azimuths, while those in blue represent the fault strike results.

involved fracture parameters using the Schoenberg linear-slide model and Hudson model. We then established the AVOA inversion equation by simplifying and rewriting the derived formula. A two-step inversion workflow was designed for the coal seam fracture parameter AVOA inversion by considering the characteristics of the AVOA inversion equation.

2) We used least-squares ellipse fitting to solve the inversion equation and determine the fracture parameters (fracture density and strike) for a target coal seam using high-density wide-azimuth pre-stack 3D seismic data. Student's *t*-distribution test was used to constrain the inversion accuracy, and the fracture density and strike inversion results showed satisfactory agreement with the fault interpretation results. Therefore, the AVOA inversion method and technical workflow proposed in this study are useful for predicting and evaluating the fracture parameters of a coal seam.

Acknowledgments We thank Yaping Huang for his comments on this manuscript. This work was supported by the University Synergy Innovation Program of Anhui Province (Nos. GXXT-2021-016 and GXXT-2019-029), the National Natural Science Foundation of China (Grant No. 41902167), and the Institute of Energy, Hefei Comprehensive National Science Center (No. 21KZS215).

References

Bakulin A, Grechka V, Tsvankin I (2000). Estimation of fracture parameters from reflection seismic data-part I: HTI model due to a single fracture set. Geophysics, 65(6): 1788–1802

Beers Y (1962). Introduction to the Theory of Error. New York: Addison Wesley Publishing Company

Chen T J, Wang X, Cui R F (2010). The detectability analysis on HTI tectonic coal cracks by azimuthal AVO's forward modeling. J China Coal Soc, 35(4): 640–644 (in Chinese)

Chen X P, Huo Q M, Lin J D, Wang Y, Sun F, Li W, Li G (2014). Theory of CBM AVO: 1. characteristics of anomaly and why it is so. Geophysics, 79(2): D55–D65

Deng X J, Peng S P, Lin Q X, Gou J W, Du W F (2010). AVO forward method of anisotropic thin coal bed. J China Coal Soc, 35(12): 2053–2058 (in Chinese)

Dong S (2004). Evaluation technique of azimuthal anisotropic cracks from P wave data and test of elastic anisotropic coefficients of coal. Dissertation for the Doctoral Degree. Xuzhou: China University of Mining and Technology (in Chinese)

Duxbury A, White D, Samson C, Hall S A, Wookey J, Kendall J M (2012). Fracture mapping using seismic amplitude variation with offset and azimuth analysis at the Weyburn CO_2 storage site. Geophysics, 77(6): B295–B306

Fu X H, Qin Y, Wei Z T (2007). Coal-Bed Methane Geology. Xuzhou: China University of Mining and Technology Press (in Chinese)

Grechka G, Tsvankin I (1998). 3-D description of normal moveout in anisotropic inhomogeneous media. Geophysics, 63(3): 1079–1092

Hall S A, Kendall J M (2003). Fracture characterization at Valhall: application of P-wave amplitude variation with offset and azimuth (AVOA) analysis to a 3D ocean-bottom data set. Geophysics, 68(4): 1150–1160

Hudson J A (1981). Wave speeds and attenuation of elastic waves in material containing cracks. Geophysical J Intern, 64(1): 133–150

Jenner E (2002). Azimuthal AVO: methodology and data examples. Leading Edge, 21(8): 782–786

Luo M, Evans B J (2003). 3D fracture assessment using AVOA and a layer-stripping approach. Explor Geophy, 34(1/2): 1–6

Luo M, Evans B J (2004). An amplitude-based multiazimuthal approach to mapping fractures using P-wave 3D seismic data. Geophysics, 69(3): 690–698

Mallick S, Craft K L, Meister L J, Chambers R E (1998). Determination of the principal directions of azimuthal anisotropy from P-wave seismic data. Geophysics, 63(2): 692–706

Mavko G, Mukerji T, Dvorkin J (1998). The Rock Physics Handbook: Tools for Seismic Analysis of Porous Media. London: Cambridge University Press

Peng S P, Chen H, Yang R, Gao Y, Chen X (2006). Factors facilitating

or limiting the use of AVA for coal-bed methane. Geophysics, 71(4): C49–C56

Peng S P, Du W F, Yin C Y, Zou G G (2014). Coal-bed gas content prediction based on AVO inversion. J China Coal Soc, 39(9): 1792–1796 (in Chinese)

Peng S P, Wang H W, Du W F, Gou J W (2013). AVO response characteristics and its influencing factors in HTI coalbed. J China Coal Soc, 38(10): 1715–1719 (in Chinese)

Ramos A, Davis T L (1997). 3-D AVO analysis and modeling applied to fracture detection in coalbed methane reservoirs. Geophysics, 62(6): 1683–1695

Rüger A (1997). P-wave reflection coefficients for transversely isotropic models with vertical and horizontal axis symmetry. Geophysics, 62(3): 713–722

Rüger A (1998). Variation of P-wave reflectivity with offset and azimuth in anisotropic media. Geophysics, 63(3): 935–947

Schoenberg M, Douma J (1988). Elastic wave propagation in media with parallel fractures and aligned cracks. Geophysical Prospecting, 36(6): 571–590

Schoenberg M, Sayers C M (1995). Seismic anisotropy of fractured rock. Geophysics, 60(1): 204–211

Shen F, Sierra J, Burns D R, Toksöz M N (2002). Azimuthal offset-dependent attributes applied to fracture detection in a carbonate reservoir. Geophysics, 67(2): 355–364

Sun W, He Z L, Li Y F, Liu Z W, Zhou Y (2014). An improved method of fracture prediction based on P-wave anisotropy and its application. Oil Geophysical Prospecting, 49(6): 1170–1178

Tian W, Zou G, Tang X M, Zeng H (2017). Method of predicting the water abundance of limestone based on AVO technique and pseudo Poisson's ratio attribute. J China Coal Soc, 42(10): 2706–2717 (in Chinese)

Wu H, Cheng Y, Zhang P, Dong S H, Huang Y P (2020). Brittleness index calculation based on amplitude variation with offset inversion for coal-bed methane reservoir: a case study of the Qinshui Basin, China. Interpretation, 8(1): SA63–SA72

Wu H, Dong S, Huang Y, Chen G W, Wang H L (2015). A method for coal structure division based on AVO simultaneous inversion. J Seismic Explor, 24(4): 365–378

Wu H, Dong S, Huang Y, Wang H, Chen G (2016). Brittleness index calculation and evaluation for CBM reservoirs based on AVO simultaneous inversion. J App Geophy, 134: 191–198

Xia G, Thomsen L, Barkved O (2006). Fracture detection from seismic P-wave azimuthal AVO analysis application to Valhall LoFS data. In: International Symposium on *In-Situ* Rock Stress, Proceedings and Monographs in Engineering, Water and Earth Sciences, 511–519